where the scope will trigger itself if the trigger condition is not met in some period of time. Auto mode is particularly useful if you are searching for some weak signal and do not want the trace to keep disappearing on you.

You have several controls on how the input voltage is handled. A "vertical position" knob on the front panel controls where the trace appears on the screen. You will find one of these for each input channel. The input "coupling" can be set to either AC, DC, or ground. In AC mode, there is a capacitor between the input connector and the vertical system circuit. This keeps any constant DC level from entering the scope, and all you see is the time-varying (i.e., AC) part. If you put the scope on DC, then the constant voltage level also shows up. If the input coupling is grounded, then you force the input level to 0, and this shows you where 0 is on the screen. (Make sure that the scope is on "auto" trigger if you ground the input; otherwise, you will not see a trace!)

Sometimes, you also get to choose the input impedance for each channel. Choosing the "high" input impedance (usually 1 MΩ) is best if you want to measure voltage levels and not have the oscilloscope interact with the circuit. However, the oscilloscope will get a lot of use looking at fast pulsed signals transmitted down coaxial cable, and you do not want an "impedance mismatch" to cause the signal to be reflected back. (See Section 3.2.1.) Cables with 50-Ω characteristic impedances are very common in this work, so you may find a 50-Ω input impedance option on the scope. If not, you should use a "tee" connector on the input to put a 50-Ω load in parallel with the input.

By flipping switches on the front, you can look at either input channel's trace separately, or both at the same time. There is obviously a problem, though, with viewing both simultaneously since the vertical trace can only be in one place at a time. There are two ways to get around this. One is to *alternate* the trace from channel one to channel two and back again. This gives complete traces of each, but does not really show them to you at the same time. If the signals are very repetitive and you are not interested in fine detail, this is okay. However, if you really want to see the traces at the same time, select the *chop* option. Here, the trace jumps back and forth between the channels at some high frequency, and you let your eye interpolate between the jumps. If the sweep speed is relatively slow, the interpolation is no problem and you probably cannot tell the difference between *alternate* and *chop*. However, at high sweep speed, the effect of the chopping action will be obvious.

You should realize by now that high-frequency operation gets hard, and the oscilloscope gets more complicated and expensive. Probably the single most important specification for an oscilloscope is its "bandwidth," and you will see that number printed on the front face right near the screen. The number tells you the frequency at which a sine wave would appear only 71% as large as it should be. You cannot trust the scope at frequencies approaching or exceeding the bandwidth. Most of the scopes in the lab have 20- or 60-MHz bandwidths. A "fast" oscilloscope will have a bandwidth of a few hundred megahertz or more. You will find that you can vary the sweep speed over a large range, but never much more than $(\text{bandwidth})^{-1}$. The "vertical sensitivity" can be set independently of the sweep speed, but scopes in general cannot go below around 2 mV/division.

On most oscilloscopes, if you turn the sweep speed down to the lowest value, one more notch puts the scope in the XY display mode. Now, the trace displays channel one (X) on the horizontal axis and channel two (Y) on the vertical. For periodic signals, the trace is a Lissajous pattern from which you can determine the relative phase of the two inputs. Oscilloscopes are also used in this way as displays for various pieces of equipment which have XY output options. Thus, the oscilloscope can be used as a plotting device in some cases.

3.3.2. Digitizers

In order to measure a voltage and deal with the result in a computer, the voltage must be *digitized*. The generic device that does this is the analog-to-digital converter or ADC. ADCs come in approximately an infinite number of varieties and connect to computers in lots of different ways. We will cover the particulars when we discuss the individual experiments, but for now we will review some of the basics.

Probably the most important specification for an ADC is its resolution. We specify the resolution in terms of the number of binary digits ("bits") that the ADC spreads out over its measuring range. The actual measuring range can be varied externally by some circuit, so the number of bits tells you how finely you can chop that range up. Obviously, the larger the number of bits, the closer you can get to knowing exactly what the input voltage was before it was digitized. A "low-resolution" ADC will have 8 bits or less. That is, it divides the input voltage up into 256 pieces and gives the computer a number between 0 and 255, which represents the voltage. A "high-resolution" ADC has 16 bits or more.

High resolution does not come for free. In the first place, it can mean a lot more data to handle. For example, if you want to histogram the voltage being measured with an 8-bit ADC, then you need 256 channels for each histogram. However, if you want to make full use of a 16-bit ADC, every histogram would have to consume 65,536 channels. Resolution also affects the *speed* at which a voltage can be digitized. Generally speaking, it takes much less time to digitize a voltage into a smaller number of bits than it does for a large number of bits.

There are three general classes of ADCs, referred to as *flash*, *peak-voltage sensing*, and *charge integrating* ADCs. A flash ADC, or "waveform recorder," simply reads the voltage level at its input and converts that voltage level into a number. They are typically low resolution, but run very fast. Today you can easily get an 8-bit flash ADC that digitizes at 100 MHz (i.e., one measurement every 10 ns). This is fast enough so that just about any time-varying signal can be converted to numbers so that a true representation of the signal can be stored in a computer.

To get better resolution, you need to decide what it is about the signal you are really interested in. For example, if you only care about the maximum voltage value, you can use a peak-sensing ADC, which digitizes the maximum voltage observed during some specified time. Sometimes, you are interested instead in the area underneath some voltage signal. This is the case, for example, in elementary particle detectors where the net charge delivered is a measure of the particle's energy. For applications like this, you can use an integrating ADC, which digitizes the net charge absorbed over some time period, i.e., $(1/R)\int_{t_1}^{t_2} V(t)\,dt$, where R is the resistance at the input. For either of these types, you can buy commercial ADCs that digitize into 12 or 13 bits in 5 μs or longer, but remember that faster and more bits costs more money.

The opposite of an ADC is a DAC, or digital-to-analog Converter. Here the computer feeds the DAC a number depending on the number of bits, and the DAC puts out an analog voltage proportional to that number. The simplest DAC has just one bit, and its output is either "on" or "off." In this case, we refer to the device as an "output register." These devices are a way of controling external equipment in an essentially computer-independent fashion.

In many cases, you want to digitize a time interval instead of a voltage level. This can be done with a "time-to-analog converter" (TAC), followed by an ADC. However, both of these functions are now available packaged in a single device called a TDC. The rules and ranges are very similar as for ADCs.

Devices known as "latches" or "input registers" will take an external logic level, and digitize the result into a single bit. These are useful for telling whether some device is on or off, or perhaps if something has happened that the computer should know about.

When a device is busy digitizing, it cannot deal with more input. We refer to the cumulative time a device is busy as "dead time." Suppose τ is the time needed to digitize an input pulse, and R_0 is the (presumably random) rate at which pulses are delivered to the digitizer. If R_m is the *measured* rate, then in a time T the number of digitized pulses is $R_m T$. The dead time incurred in time T is therefore $(R_m T)\tau$, so the number of pulses lost is $[(R_m T)\tau]R_0$. The total number of pulses delivered $(R_0 T)$ must equal the number digitized plus the number lost, so

$$R_0 T = R_m T + R_m T \tau R_0,$$

and therefore

$$R_m = \frac{R_0}{1 + \tau R_0} \tag{3.13}$$

or

$$R_0 = \frac{R_m}{1 - \tau R_m}. \tag{3.14}$$

The "normal" way to operate a digitizer is so that it can keep up with the rate at which pulses come in. In other words, the rate at which it digitizes $(1/\tau)$ should be much greater than the rate at which pulses are delivered, that is, $\tau R_0 \ll 1$. Equation (3.13) shows that in this case, $R_m \approx R_0$; that is, the measured rate is very close to the true rate, which is just what you want. Futhermore, an accurate correction to the measured rate is given by Eq. (3.14), which can be written as $R_0 = R_m(1 + \tau R_m)$ under normal operation.

On the other hand, if $\tau R_0 \gg 1$, then $R_m \approx 1/\tau$. That is, the digitizier measures a pulse and before it can catch its breath, another pulse comes along. The device is "always dead," and the measured rate is just one per digitizing time unit. Essentially all information on the true rate is lost, because the denominator of Eq. (3.14) is close to 0. You would have to know the value of τ very precisely in order to make a correction that gives you the true rate.

8.2.5. Passage of Electromagnetic Radiation (Photons) through Matter

As mentioned in the introduction to this section photons lose energy or are absorbed in matter by one of the following three mechanisms:

(a) Photoelectric effect, which predominates at low energies,
(b) Compton effect, which predominates at medium energies (below a few MeV), and
(c) Pair production of electrons and positrons, which is dominant in the high-energy region.

The relative importance of these processes and the energies at which they set in are best seen in Fig. 8.7, which gives the cross section for the interaction of a photon as a function of its energy (in units of the electron's rest mass). We will now briefly consider each process separately.

(a) *Photoelectric Effect.* We speak of the photoelectric effect when the photon is completely absorbed and all its energy is transferred to an atomic electron. Consequently the photon must have enough energy to excite the bound electron from its quantum state to a higher state or into the continuum; the latter process (ionization of the atom) is much more probable. Since the binding energy of the inner electrons in atoms is on the order of kiloelectronvolts, as the frequency of the photon is increased and it reaches the value of the binding energy of a particular shell,[13] a new "channel" opens, and we expect a sudden rise in the absorption cross section. Apart from the onset of new channels, the overall variation of the photoelectric effect is a rapid decrease as the third power of the photon frequency (as $\nu^{-7/2}$), thus resulting in the curve shown on the left in Fig. 8.7. The cross section for the photoelectric effect is derived in Heitler (1954),[14] from which we give the nonrelativistic value for the ejection of *one* electron from the K shell, when the photon energy is not too close to

[13]Note that $n = 1$ electrons are said to be in the K shell, $n = 2$ in the L shell, $n = 3$ in the M shell, etc.

[14]W. Heitler, *The Quantum Theory of Radiation*, 3rd ed., pp. 207 and 208, Oxford Univ. Press, Oxford, 1984.

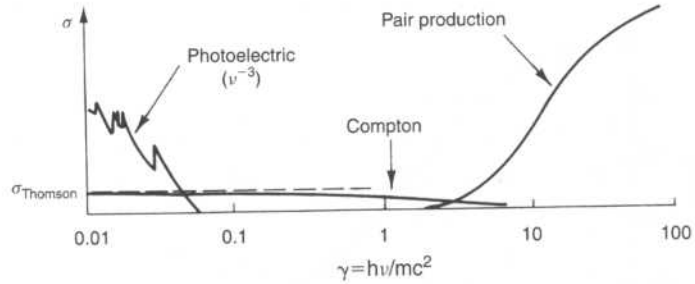

FIGURE 8.7 The cross section for the interaction of photons with matter as a function of their energy (expressed in units of the electron's rest mass).

the absorption edge,

$$\sigma_P = \sigma_T \frac{Z^5}{(137)^4} 2\sqrt{2} \left[\frac{h\nu}{mc^2}\right]^{-7/2} \text{(cm}^2\text{)}. \tag{8.20}$$

Note the dependence on the Z of the nucleus, indicating that L shell and higher-shell ejection is less probable because of the screening of the nuclear charge. Here σ_T is the classical Thomson cross section, which is derived from the simplified assumption of a plane polarized elecromagnetic wave scattering from a free electron (it is assumed that the displacement of the electron is much smaller than the wavelength); we obtain

$$\sigma_T = \frac{8\pi}{3}\left[\frac{e^2}{mc^2}\right]^2 = \frac{8\pi}{3} r_0^2, \tag{8.21}$$

where $r_0 \equiv e^2/mc^2$ is the classical radius of the electron $= 2.8 \times 10^{-13}$ cm. Note that the Thomson cross section is independent of the frequency of the incoming photon.

(b) *Compton Effect.* In the Compton effect, the photon scatters off an atomic electron and loses only part of its energy. This phenomenon, which is one of the most striking quantum effects, is described in detail in Section 9.2; the cross section for Compton scattering is given by the Klein–Nishina (K–N) formula, shown in an expanded scale in Fig. 8.8. The energy of the photon is given on the abscissa in units of the electron rest mass[15] $\gamma = h\nu/mc^2$, and the ordinate gives the ratio of the Compton cross section σ_C to the classical Thomson cross section σ_T.

[15]Not to be confused with the usual definition of γ for a charged particle $\gamma = E/mc^2$, introduced in Eq. (8.13).

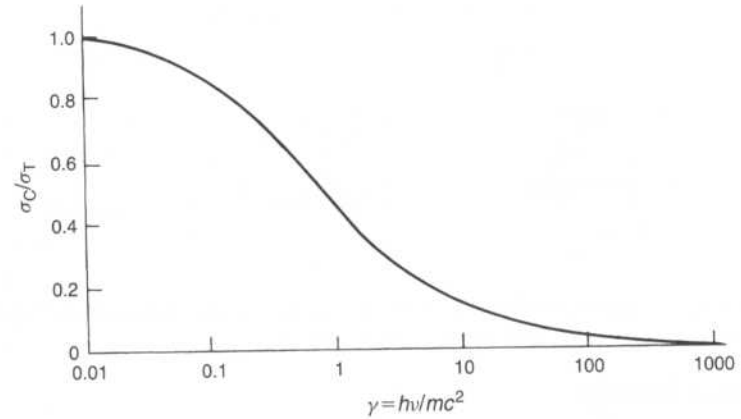

FIGURE 8.8 The ratio of the Compton scattering cross section, σ_C, to the constant Thomson cross section, σ_T, as a function of photon energy expressed in units of the electron's rest mass.

We give below the asymptotic approximations to the (K–N) Compton scattering cross section:

For low energies:

$$\sigma_C = \sigma_T \left(1 - 2\gamma + \frac{26}{5}\gamma^2 + \cdots\right) \qquad \gamma = h\nu/mc^2 \ll 1$$

For high energies:

$$\sigma_C = \frac{3}{8}\sigma_T \frac{1}{\gamma}\left(\ln 2\gamma + \frac{1}{2}\right) \qquad \gamma = h\nu/mc^2 \gg 1. \tag{8.22}$$

(c) *Pair Production.* In pair production a photon of sufficiently high energy is converted into an electron–positron pair. For a free photon conservation of energy and momentum would not be possible in this process, so pair production must take place in the field of a nucleus (or of another electron), which will take up the balance of momentum. Clearly the threshold for this process is $2mc^2$ (where m is the mass of the electron), hence 1022 keV. The cross section for pair production rises rapidly beyond the threshold, and reaches a limiting value for $h\nu/mc^2 \approx 1000$ given by[16]

$$\sigma_{\text{pair}} = \frac{Z^2}{137} r_0^2 \left[\frac{28}{9} \ln \frac{183}{Z^{1/3}} - \frac{2}{27}\right] \quad (\text{cm}^2). \tag{8.23}$$

[16] See Heitler (1984), p. 260.

Since both the photoelectric and Compton effect cross sections decrease as the photon energy rises, pair production is the predominant interaction mechanism for very high-energy photons.

It is advantageous to introduce the mean free path (L_{pair}) for pair production; when a photon traverses a material with density of nuclei n,

$$L_{\text{pair}} = \frac{1}{n\sigma_{\text{pair}}} = \frac{1}{(28/9)(Z^2 n/137) r_0^2 \ln(183/Z^{1/3})}, \tag{8.24}$$

where we have dropped the small term 2/27. Thus, the attenuation of a beam of I_0 photons will proceed as

$$I(x) = I_0 e^{-x/L_{\text{pair}}}. \tag{8.25}$$

In conclusion, Fig. 8.9 gives the total absorption coefficient for a photon traversing lead as a function of its energy (in units of the electron rest mass). Note that

$\kappa_P = \sigma_P 2n$	because there are 2 K-shell electrons per nucleus
$\kappa_C = \sigma_C n_e$	electron density
$\kappa_{\text{pair}} = \sigma_{\text{pair}} n$	density of nuclei.

The dashed curves in Fig. 8.9 indicate the relative contributions of each of the three interaction mechanisms.

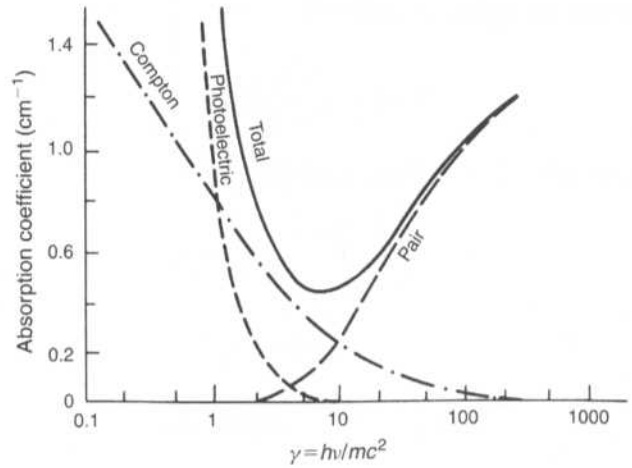

FIGURE 8.9 The relative contribution of the three effects responsible for the interaction of photons with matter. The absorption coefficient in lead is plotted against the logarithm of photon energy (in units of the electron's rest mass).

This phenomenon of recovery can be clearly seen in Fig. 8.19, obtained by a student. The Geiger counter was exposed to a high flux of radiation; the trace of an oscilloscope is triggered when the output pulse appears. The horizontal scale is 100 μs/cm so that the shape of the output pulse and its exponentially decaying tail can be seen in detail. If now a second particle arrives within 1 ms of the previous one, it will appear on the same oscilloscope trace since the scope will not trigger again until the sweep is completed (the screen is 10 cm wide). The picture shown in Fig. 8.19 was obtained by making a multiple exposure of such traces. The correlation of pulse height against delay in arrival time and the exponential dependence of the recovery are clearly noticeable. If we consider that the counter is inoperative until the output is restored to 63% of its original value $(1-1/e)$, the data of Fig. 8.19 give a value for the dead time τ on the order of

$$\tau = 400\ \mu\text{s}. \tag{8.39}$$

Pulses, however, seem to appear after an interval

$$\tau \approx 300\ \mu\text{s}. \tag{8.40}$$

The dead time of a counter may also be obtained by an "operational" technique, such as by measuring the counting loss when the detector is subjected to high flux. If the dead time is τ (s), and the counting rate R (counts/s), the detector is inoperative for a fraction $R\tau$ of a second; the true counting efficiency is then $1 - R\tau$.

Consider two sources S_1 and S_2, which when placed at distances from the counter D_1 and D_2 give a true rate (counts/s) R_1, R_2. The counter, however, registers rates $R_1' < R_1$, $R_2' < R_2$ due to dead-time losses, and when both sources are simultaneously present, it registers $R_{12}' < R_1' + R_2'$ due to the additional loss accompanying the higher flux. Now,

$$\begin{aligned} R_1' &= R_1(1 - R_1'\tau) \\ R_2' &= R_2(1 - R_2'\tau) \\ R_{12}' &= (R_1 + R_2)(1 - R_{12}'\tau). \end{aligned}$$

We solve by writing

$$\frac{R_{12}'}{1 - R_{12}'\tau} = \frac{R_1'}{1 - R_1'\tau} + \frac{R_2'}{1 - R_2'\tau},$$

which reduces to a quadratic equation in τ with the solution

$$\tau = \frac{1 \pm \sqrt{1 - R_{12}'(R_1' + R_2' - R_{12}')/R_1'R_2'}}{R_{12}'}.$$

This can be expanded in the small quantity $(R_1' + R_2' - R_{12}')$ to give the approximate expression

$$\tau \approx \frac{(R_1' + R_2' - R_{12}')}{2R_1'R_2'}. \tag{8.41}$$

We now apply Eq. (8.41) to data obtained by students with the same counter used for Fig. 8.19. In practice, source S_1 is first brought to the vicinity of the counter and R_1' is obtained, next S_2 is also brought in the area and R_{12}' is obtained, and finally S_1 is removed and R_2' is measured: thus no uncertainties due to source position can arise. They obtain

$$\begin{aligned} R_1' &= 395 \pm 3\ \text{counts/s} \\ R_{12}' &= 655 \pm 3\ \text{counts/s} \\ R_2' &= 334 \pm 3\ \text{counts/s}, \end{aligned}$$

yielding $\tau = 282 \pm 20\ \mu\text{s}$, in better agreement with Eq. (8.40) than with Eq. (8.39).

The rather long dead time of the Geiger counter is a serious limitation restricting its use when high counting rates are involved; the ionization counter and proportional counter have dead times several orders of magnitude shorter.

8.4. THE SCINTILLATION COUNTER

8.4.1. General

As we saw, in gaseous-ionization instruments, the electron–ion pairs were directly collected; in the scintillation counter the ionization produced by the passage of a charged particle is detected by the emission of weak scintillations as the excited molecules of the detector return to the ground state. The fact that certain materials emit scintillations when traversed or struck by charged particles has been known for a long time, Rutherford being the first to use a ZnS screen in his alpha particle scattering experiments.

The scintillation counters used currently were developed in the 1950s and consist of an organic or inorganic crystal coupled to a sensitive photomultiplier that responds to the light pulses. Anthracene or stilbene crystals make excellent scintillators, but organic compounds embedded in transparent plastic, such as polystyrene, are now widely used because of ease in handling and machining and availability in large sizes. Such materials are commercially available[31] under the general description of "plastic scintillators." The active materials are compounds, such as "PPO," 2-5-diphenyloxazole, or diphenylstilbene, or others, and are also available in liquid form.

Organic scintillators have an extremely fast response, on the order of 10^{-9} s, which can be matched by good photomultipliers. On the other hand, because of the low density and low Z, their efficiency for gamma-ray conversion is not high. To detect gamma rays, inorganic crystals, such as NaI or CsI, are used instead, activated with some impurity, for instance Tl (1 part in 10^3). Inorganic crystals have an excellent efficiency for gamma-ray conversion, due to their high Z; from Eq. (8.20) we recall that the photoelectric effect is proportional to Z^5 and from Eq. (8.23) pair production is proportional to Z^2. However, the light output from inorganic crystals is spread over a much longer time interval, on the order of 10^{-6} s. Such inorganic crystals are also available commercially,[32] appropriately encased since they are damaged by humidity; they come in sizes up to several cubic inches.

The light output of scintillators is proportional (as a matter of fact, linear) to the energy lost by the particle that traverses the detector; thus, by pulse-height analyzing the electrical output of the photomultiplier, the scintillation counter may be used as a spectrometer. This procedure is discussed in detail in the following section, where it is seen that energy resolution on the order of 10% or better is achievable.

The mechanism of emission of the photons in the scintillator material is rather involved. Table 8.2 gives a chart of the processes involved in the emission of light in organic and inorganic crystals. In inorganic materials it is the migration of the electrons through the lattice (until they excite an impurity center) that is responsible for the long duration of the light pulse.

Even though the efficiency for transferring the energy lost by ionization to the photons in the visible region is on the average low, $\epsilon \approx 1.5\%$, a scintillator still provides ample light output. Consider the case of a plastic scintillator 1-cm thick, traversed by a minimum-ionizing particle: $dE/dx = 2 \times 10^6$ eV per g/cm^2; if we take the average photon energy

[31] For example, from Pilot Chemicals Inc., 36 Pleasant St., Watertown, MA.

[32] For example, from Harshaw Chemical Corp., Cleveland, OH.

TABLE 8.2 The Series of Processes Leading to the Emission of Light When a Charged Particle Traverses a Scintillator Material[a]

Inorganic scintillator	Organic scintillator
(Impurity activated)	Electronic structure of molecule is excited → Loss of energy to vibrational states → Emission of light quantum
Holes → Drift to impurity center and ionize it. Emission of thermal radiation	Electrons → Capture with emission of thermal radiation
Ionized impurity center → Excited impurity center → Emission of light quantum	Dissociation
Electron drops into metastable state of impurity center → Thermal energy raises electron to excited state	Energy may be transferred to other molecules → Radiationless transition
Radiationless transition	

[a] After J. Sharpe, *Nuclear Radiation Detectors*, Methuen, London, 1965 (Courtesy of the Publishers).

as 3 eV, we obtain 10^4 photons. The efficiency of a photomultiplier cathode for converting photons into electrons is on the order of 0.1, and the geometric efficiency for collecting the photons onto the photocathode is usually high, so that on the order of 1000 electrons are released. With modern techniques, however, it is possible to detect the release of a few photoelectrons, or even of a single one.

Clearly the scintillator material must be transparent to the visible radiation and optical coupling to the photomultiplier must be provided. This is achieved either directly or through a "lightpipe," which is an appropriately shaped piece of lucite or other medium of high refractive index that traps and guides the light due to total internal reflection at its surfaces. At the surfaces where the lightpipe is joined to the scintillator or to the photomultiplier, optical contact is achieved by the use of either viscous fluids or special glues.[33] Obviously the whole assembly must be light tight; this is frequently achieved by wrapping black electrical tape around the scintillator, lightpipe, and phototube.

Because of its great stability and ease of operation, as well as because of its time and energy resolution, the scintillation counter has become the most frequently used detector in nuclear physics, especially for high-energy particles.

8.4.2. Experiment on the Determination of the Energy of Gamma Rays with a Scintillation Counter

If atoms are quantum-mechanical systems and a typical manifestation of this fact is the emission of spectral lines of light, it should be expected that nuclei, when excited, would emit similar line spectra.

Since the nuclear radius is three to five orders of magnitude smaller than that of atoms, the forces that bind the nucleus (against the repulsion of the positive charges confined in its volume) must be correspondingly stronger than the forces that bind the atomic electrons to the nucleus. As a consequence, the energy levels and the quanta of energy emitted in a nuclear transition are also orders of magnitudes larger than those of atomic transitions. Indeed, the quanta of electromagnetic radiation emitted in a nuclear transition fall in the gamma-ray region, and new techniques are needed for their detection and for the measurement of their (wavelength) energy.

[33] In the first category, Corning 200,000 centipoise fluid or clear vacuum grease; in the latter, R 363, PS 28 acrylic glue, etc.

Further, because of the larger spacing between energy levels, it is not easy to excite a nucleus from its ground state by the simple means of electric discharges or arc sources such as are used for atoms; instead, beams of neutrons or high-energy gamma rays, or high-energy charged particles, are required. However, in distinction to atomic transitions where the de-excitation probability is on the order of 10^8/s, some nuclear transitions have a very small "decay" probability, as small as 10^{-7}/s, corresponding to a lifetime of 100 days. Thus, it is possible to excite a sample of nuclei inside a nuclear reactor, or by subjecting them to cyclotron bombardment, or by other means, and subsequently bring them to the laboratory for measuring their spectrum or for other uses. Indeed, some of the nuclei that have very long lifetimes can be found in nature in their excited state; these are the naturally radioactive elements.

We now know that the appropriate detector for measurements of the energy of gamma rays is an inorganic crystal. When a gamma ray of energy <1 MeV enters the detector, it will interact either by the photoelectric effect or the Compton effect. In the former case it is fair to assume that the ejected photoelectron will deposit all its energy in the scintillator; in the Compton effect, however, the scattered photon may or may not convert in the scintillator (depending on the size and geometry of the detector).

The pulse-height spectrum for gamma rays of a given energy will consist of a peak at an energy corresponding to that of the gamma ray and a continuum below the peak, corresponding to Compton-scattered gamma rays that escaped from the crystal before totally converting. This can be seen in Fig. 8.20 and those that follow. Clearly the larger the size of the crystal, the larger the percentage of the output counts that will lie in the photopeak; thus, the gamma-ray line will become more pronounced.

Most of the data reported here were obtained with a NaI–Tl activated crystal,[34] 2 in. in diameter and 2 in. wide, coupled directly to a photomultiplier tube.[35] (Photomultiplier tubes and high-voltage bias schemes are discussed in Appendix E.2.) The output pulse is fed to an Ortec[36] Model 570 amplifier, and its output is fed to a Canberra multiport multichannel analyzer (MCA). The MCA is controlled and read out through a

[34] Bicron Corporation, http://www.bicron.com/.

[35] The crystal and photomultiplier tube assembly is a commercial package from Canberra Industries, http://www.canberra.com/, Model 802-3. The photomultiplier tube "base" was constructed from a commercial socket and simple components.

[36] http://www.ortec-online.com/.

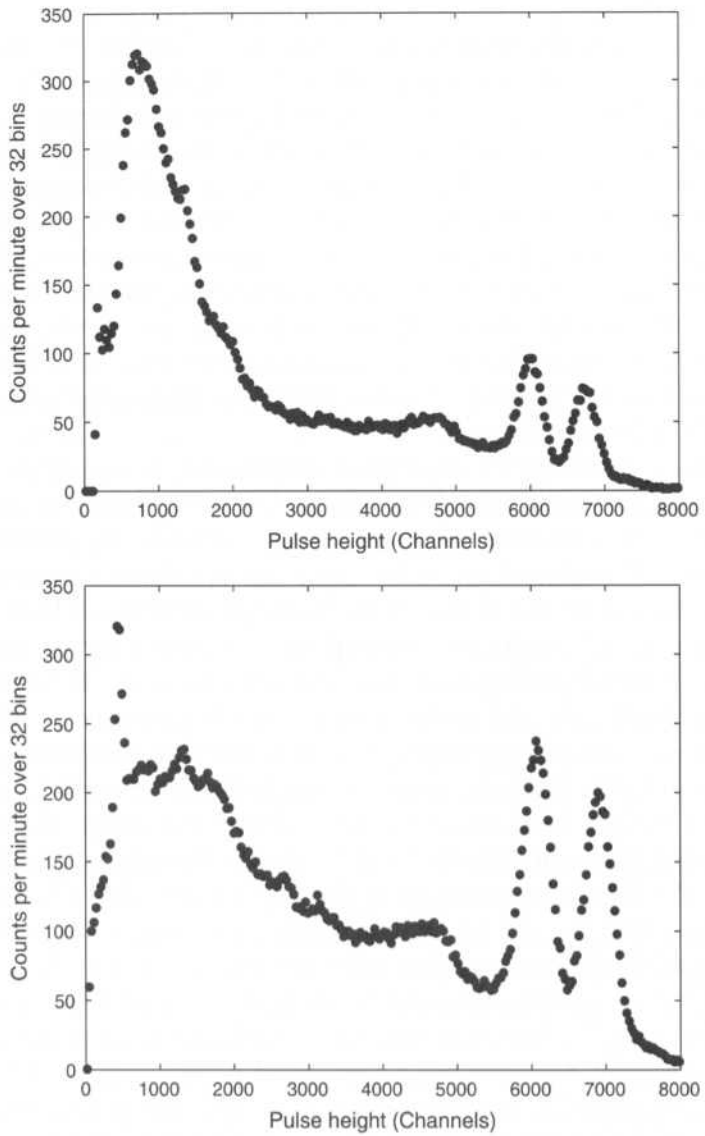

FIGURE 8.20 Pulse-height spectrum of ^{60}Co gamma rays obtained with a NaI crystal, along with the decay scheme of ^{60}Co. The upper spectrum was taken with a 2-in.-diameter crystal detector, while the bottom was taken with a 3-in. crystal. The ^{60}Co source was relatively weak (less than 1 μCi when these data were taken) and the source-to-detector distance was 10 cm. The decay scheme is also shown.

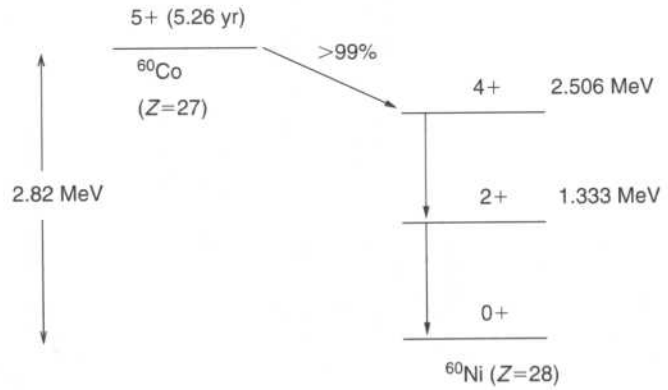

FIGURE 8.20 (*Continued*)

GPIB interface, in this case using a laptop computer. Spectra acquired in this way are histograms with $8192 = 2^{13}$ bins. (Adjacent bins were added together to reduce the statistical fluctuations from bin to bin. This is easy to do with the `reshape` command in MATLAB.) The conversion of bin number to photon energy depends on the combined gain of the photomultiplier and the amplifier, and must be calibrated with sources of known photon energy.

The following figures give the results obtained by a student. Figure 8.20 gives the spectrum of ^{60}Co and shows two distinct peaks, which we attribute to gamma rays emitted in the de-excitation of ^{60}Ni from its 2.505-MeV level to the 1.333-MeV level, and from that level to the ground state according to the decay scheme also shown in the figure. For comparison, we also show a spectrum taken with a 3-in.-diameter and 3-in.-wide crystal. As a measure of the energy resolution, we may consider the full-width of the peak at half-maximum, which is on the order of 480 channels, hence a resolution of $480/6000 \approx 8\%$. We also notice a significant background for pulse heights lower than that of the peaks, which is due to Compton-scattered gamma rays that subsequently escaped from the crystal. This background is much less severe for the larger crystal.

Figure 8.21 gives similar data for a sample of ^{137}Cs; here the 0.662-MeV gamma ray represents the de-excitation of ^{137}Ba. Again we notice some Compton background and an energy resolution on the order of 10%. Figures 8.22 and 8.23 give the pulse-height spectra from ^{22}Na and ^{133}Ba, respectively. For the ^{22}Na, the peak at 1.277 MeV arises from the de-excitation of ^{22}Ne; the larger peak at 0.511 MeV arises from annihilation radiation. Indeed, from the level diagram of ^{22}Na decay, we notice that

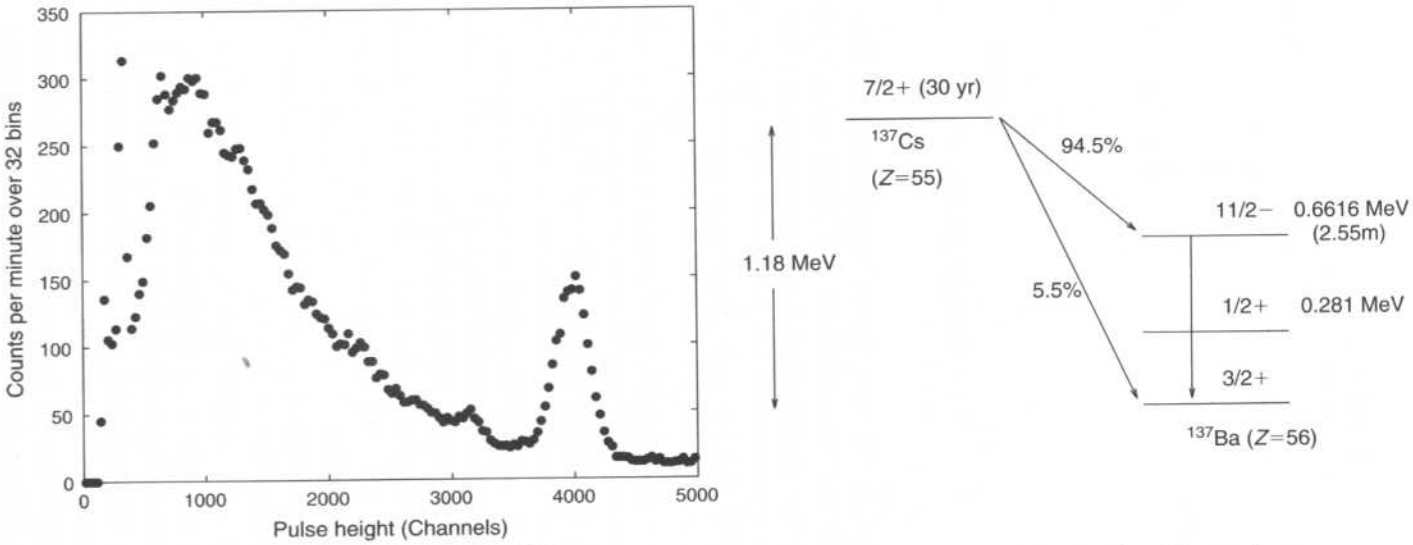

FIGURE 8.21 Pulse-height spectrum of ^{137}Cs gamma rays obtained with a NaI crystal, and the associated decay scheme.

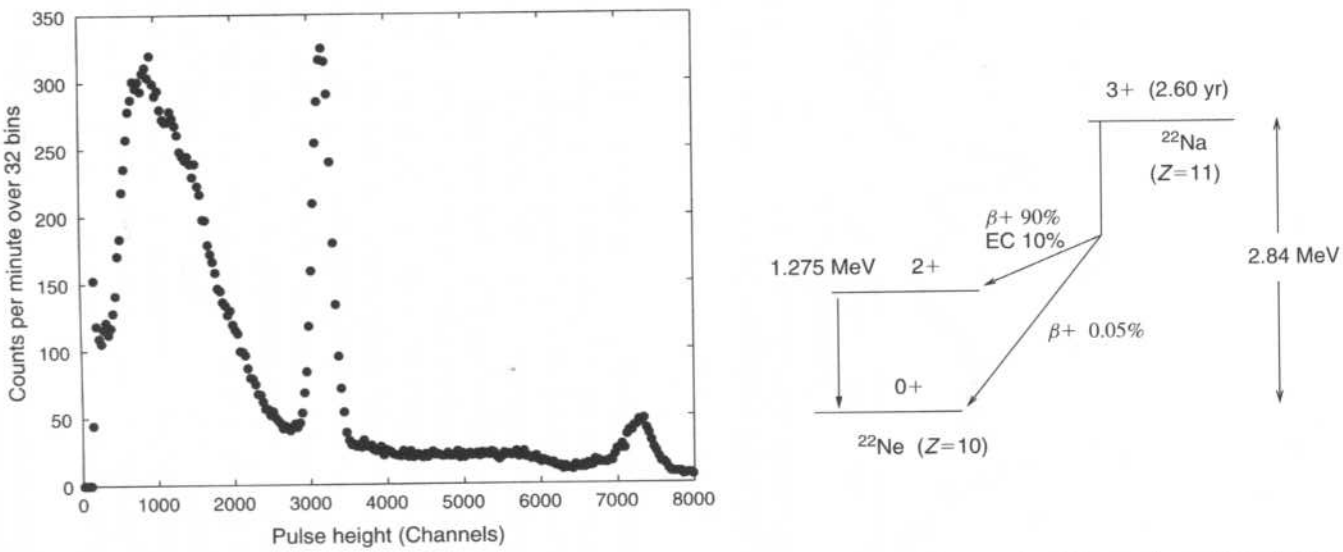

FIGURE 8.22 Pulse-height spectrum of ^{22}Na gamma rays obtained with a NaI crystal, and the associated decay scheme. Note that the 511-KeV line is due to positron annihilation.

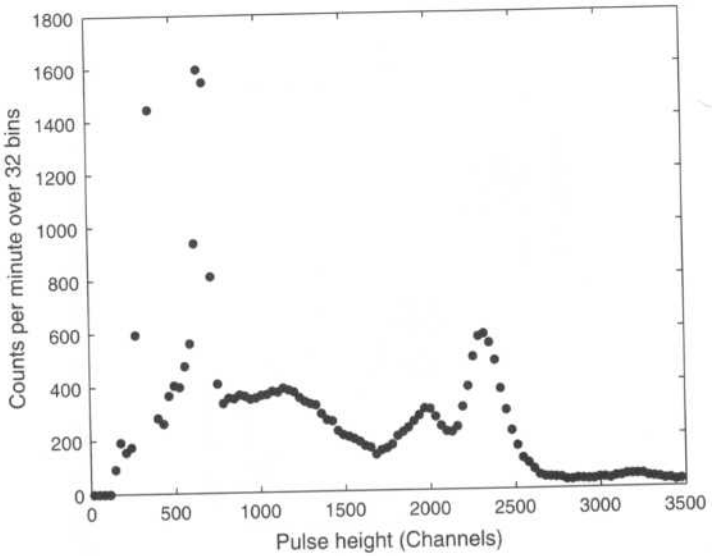

FIGURE 8.23 Pulse-height spectrum of ^{133}Ba gamma rays obtained with a NaI crystal. The decay scheme is complicated, but the most dominant γ rays at high energy are at 356 and 302 keV.

positrons are emitted; the positrons are usually stopped in the walls of the source container, or in the crystal face, and as they come close enough to an electron they annihilate into two gamma rays, each gamma ray sharing the energy of the electron–positron pair.[37] It is *one*[38] of these gamma rays that is then converted in the crystal and gives rise to the 0.511-MeV peak.

Finally, in Fig. 8.24 is given a plot of all the observed peaks against channel number, showing the linearity of pulse height against energy. (MATLAB provides a useful utility command, ginput, for interactively identifying the peak position in spectrum plots using the cursor on your computer.) In addition to the gamma rays, the nuclei investigated also emit beta rays, and one would expect to see the corresponding peaks in the pulse-height spectrum. This, however, is not true because the beta spectrum is continuous instead of being a sharp line as is the case with gamma-ray spectra; in addition, electrons may lose variable amounts of energy before reaching the scintillation crystal, so that unless special precautions are taken, the energy resolution is usually poor.

[37] See also the detailed discussion in Chapter 9.

[38] Note that they are emitted with a relative angle of 180°.

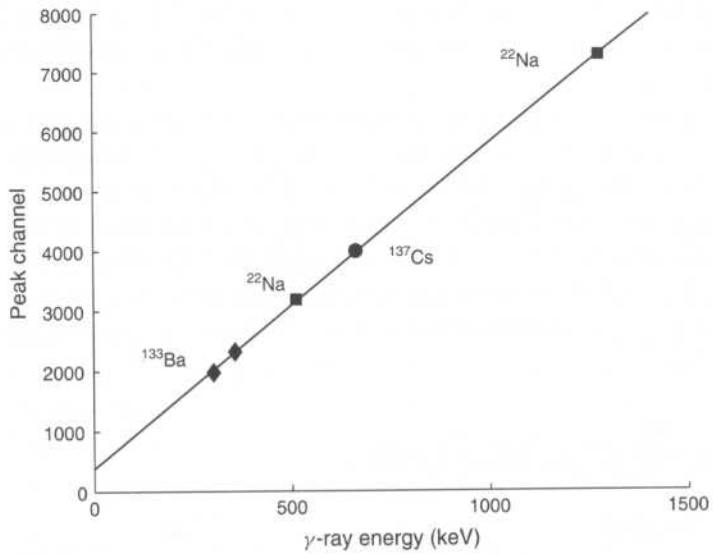

FIGURE 8.24 Plot of gamma-ray energy against the central channel of the photopeak appearing in the spectra of Figs. 8.21 through 8.23. The detector response is obviously qui linear over this range. Note also that for a zero photon energy, there is a "pedestal" of few hundred channels. This ensures that none of the spectrum is lost below the range of th multichannel analyzer.

In interpreting gamma-ray spectra some care must be taken since spu rious peaks due to instrumental effects or physical effects do appea First, there can be peaks arising from the emission of X-rays, followin photoejection of K-shell electrons either in the source or in the shieldin Also, a peak may appear due to photons that backscatter (by 180°) in th photomultiplier window or elsewhere; then the Compton-scattered elec tron escapes, but the scattered photon becomes converted in the crysta For ^{137}Cs with its 0.662-MeV gamma ray, the backscattering peak appea at 0.185 MeV and can be identified in a carefully measured spectrum.

Another spurious effect occurs when an incoming photon of energy ejects a K-shell electron from the iodine of the crystal, but the emitted X-ra escapes without converting in the detector. The ejected photoelectron ha an energy

$$E - E_K,$$

where E_K is the energy of the K shell of iodine, namely, 29 keV, and wi give rise to a peak not coinciding with the true photopeak. This so-calle

"escape-peak" can be identified because it is located 29 keV below the photopeak; it is most pronounced in the pulse-height spectra of low-energy gamma rays.

The relative ratio of counts in the photopeak as compared to the counts in the Compton background depends on the crystal and source geometry and on the gamma-ray energy. Usually the relative counts in the photopeak give sufficient information, but when the absolute number of gamma rays is required, we must calculate the efficiency of the crystal for the particular geometry and gamma-ray energy. Extensive tables of efficiency for most combinations of the relevant parameters have been calculated.[39]

8.5. SOLID-STATE DETECTORS

8.5.1. General

We have seen how the gaseous ionization counters and the scintillation counters are widely used for the detection of radiation and charged particles. It is also possible to use semiconductor materials for the detection of charged particles, especially those of low energy; such detectors are appropriately referred to as "solid-state counters."[40]

In a general sense, we can think of this type of detector as a solid-state ionization chamber, having two basic advantages over a gas-filled ionization chamber:

(a) The energy required for the creation of an electron–ion pair is 3 eV (as compared to approximately 30 eV in a gas) so that stronger signals and better statistics can be achieved.

(b) The stopping power is approximately 10^3 times that of a gas-filled device (since the detector material is so much denser), and thus it becomes possible to stop, in the *detector*, particles with energies typical of nuclear interactions. Consequently a very large number of electron–ion pairs are formed, leading to very good energy resolution. A 1-MeV proton stopping in a solid-state detector will create 300,000 electron–ion pairs, while the same proton traversing a proportional counter of 2-cm thickness would only release approximately 30 pairs.

[39] See the *Encyclopedia of Physics*, Vol. 45, *Nuclear Instrumentation II*, p. 110.

[40] The scintillation counter is also a detector in the solid state!

In practice, however, it must be possible to collect the free charges (those created by the passage of the charged particle) before they recombine; this might be done, for example, by the application of an electric field in the detector material. This requirement is very difficult to meet with any of the ordinary crystals. Clearly, the material must have a high resistivity, since otherwise current will flow under the influence of the field, masking the effect of the pulse produced by the passage of the particle; on the other hand, in high-resistivity materials, the mobility of the free carriers is very low and the recombination probability high.

Even though some results have been obtained by using diamond as a detector, semiconductor materials come much closer to fulfilling the requirements mentioned above. Very pure material (an intrinsic semiconductor) is used to achieve the necessary high resistivity, on the order of 10^7 Ω-cm, and the detector is operated at low temperatures. Such devices are called "bulk semiconductor detectors."

A great improvement occurs when a semiconductor junction[41] is used as the detector volume; a device of this kind is called a barrier-layer detector. The junction is made by either of the following methods:

(a) Diffusing a high concentration of *donor* impurities on a p-type material, usually silicon, thus creating an n–p junction.

(b) Utilizing a thin p-type surface formed by oxidizing n-type silicon or germanium when it is exposed to air. This surface is so thin that it is usually coated with gold to provide a good electrical contact; thus we have a p–n junction.

In either case the operation is similar, but the junction is always reverse biased.

Below we will briefly discuss the diffused junction (n–p) type of detector; Fig. 8.25a is a reproduction of Fig. 2.20, and gives the configuration of the energy bands at an n–p junction, electrons being the majority carriers in the left, or n, region, and holes the majority carriers in the right, or p, region. Electrons may not move to the right, since the conduction band is at a higher (negative) potential, and holes may not move to the left, since the valence band is now at a higher (positive) potential; as a consequence there is some *repulsion* of *majority* carriers from the junction; Fig. 8.25b shows their density distribution. We note a "depletion zone" in the region marked $S-T$.

[41] Semiconductor junctions were discussed in 2.4.2, and the reader may find it useful to review that material.

CHAPTER 9

Scattering and Coincidence Experiments

9.1. INTRODUCTION

Ever since Rutherford performed his original experiments on the scattering of energetic alpha particles from atomic nuclei, scattering has become increasingly more powerful as a tool for investigating the forces between elementary particles. By now it is familiar to the reader that an electron, under the influence of the attractive electromagnetic force of the nucleus, may be found in a bound state. The classical analogue of this situation is the motion of the planets around the sun under the influence of the gravitational force; they describe elliptical orbits.

In general, a scattering experiment probes a system by sending a projectile "into" it, and then studying what "comes out" of it. Similarly, correlation or "coincidence" experiments can probe a system by looking at what comes out simultaneously in two or more directions. In this chapter, we will study some types of each of these measurements.

The experiments in this chapter make use of radioactive sources. We recommend that the reader review the material on radiation safety in Appendix D before undertaking these measurements.

The concept of "solid angle" is important for understanding the formalism dealing with cross sections. The solid angle is a three-dimensional generalization of the familiar planar angle $\Delta\theta$, which is the length of a circular arc Δs divided by the radius r of the circle, i.e., $\Delta\theta = \Delta s/r$. Solid angle $\Delta\Omega$ is the area ΔA of a piece of a spherical surface, divided by the square of the radius, i.e., $\Delta\Omega = \Delta A/r^2$. Planar angles are measured in radians and solid angles are measured in steradians. Just as a circle subtends a planar angle of 2π to any point included in the circle, a sphere subtends a solid angle of 4π to any included point.

Solid angle is a useful concept whenever we are dealing with some sort of detector intercepting radiation which spreads out in all directions from a source. Ionizing radiation and elementary particle detectors are just one example, but you would encounter the same thing in fields like optics or sonics.

To be explicit, let $d\mathbf{A}$ be a vector whose magnitude is an area dA in some plane, and whose direction is normal to that plane. Let $\mathbf{n}$ be a unit vector pointing toward the source, which is a distance r away. Then

$$d\Omega = \frac{\mathbf{n}\cdot d\mathbf{A}}{r^2} \equiv \frac{dA_\perp}{r^2}, \tag{9.1}$$

where $dA_\perp$ is just the perpendicular component of the area. A spherical surface is most convenient since all surface elements are normal to the direction to the center. In spherical coordinates (r, θ, ϕ), where $0 \le \theta \le \pi$ is the polar angle and $0 \le \phi \le 2\pi$ is the azimuthal angle, a differential element of the surface has area

$$dA = \text{width} \times \text{height} = (r\sin\theta\, d\phi) \times (r\, d\theta) = r^2 \sin\theta\, d\theta\, d\phi,$$

so the infinitesimal solid angle is just

$$d\Omega = \sin\theta\, d\theta\, d\phi. \tag{9.2}$$

You will encounter this equation many times in physics.

We can easily apply this to the common case of a "detector face," normal to the direction of the incident radiation, as shown in Fig. 9.1. Let the "detector face" be a circular area with radius R located a distance d from a source. There is perfect azimuthal symmetry, so we immediately integrate

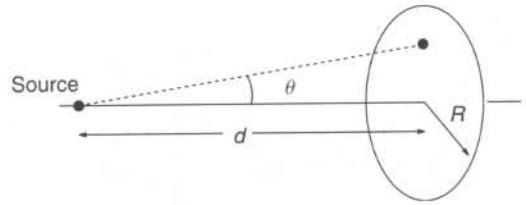

FIGURE 9.1 Calculating the solid angle of a circular face.

over ϕ to get

$$d\Omega = 2\pi \sin\theta\, d\theta$$

and integrate from $\theta = 0$ to $\theta_{\max} = \tan^{-1}(R/d)$ to get

$$\frac{\Delta\Omega}{4\pi} = \frac{1}{2}\int_{\theta=0}^{\theta_{\max}} \sin\theta\, d\theta,$$

where we have written the fraction of the total solid angle as $\Delta\Omega/4\pi$. This integral is done most easily by a change of variables to $\mu = \cos\theta$ with μ ranging from $\cos\theta_{\max} = d/\sqrt{d^2 + R^2}$ to 1. Since $d\mu = -\sin\theta\, d\theta$,

$$\frac{\Delta\Omega}{4\pi} = \int_{\cos\theta_{\max}}^{1} d\mu = \frac{1}{2}\left[1 - \frac{d}{(d^2 + R^2)^{1/2}}\right]. \tag{9.3}$$

For $d = 0$, $\Delta\Omega/4\pi = 1/2$, that is, the surface covers one entire hemisphere. For $d \to \infty$, expand Eq. (9.3) to first order in R/d to find $\Delta\Omega/4\pi = R^2/4d^2$ or $\Delta\Omega = (\pi R^2)/d^2$, which is just what you expect from the basic definition of solid angle.

9.2. COMPTON SCATTERING

9.2.1. Frequency Shift and Cross Section

This section deals with the scattering of electromagnetic radiation by free electrons. As mentioned in the introduction to this chapter, it is the scattering of electromagnetic radiation from various objects that makes it possible for us to "see" them. However, as the frequency of the radiation is increased beyond the visible region, the light quanta have energies comparable to, or larger than, the binding energy of the electrons in atoms, and the electrons can therefore be considered as free.

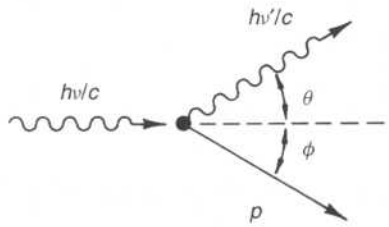

FIGURE 9.2 Compton scattering of a photon from a free electron.

In 1920 A. H. Compton investigated the scattering of monochromatic X-rays from various materials. He observed that after the scattering, the energy (frequency) of the X-rays had changed, and had always decreased. From the point of view of classical electromagnetic theory, this frequency shift cannot be explained,[1] since the frequency is a property of the incoming electromagnetic wave (field) and cannot be altered by the change of direction implied by the scattering. If, on the other hand, we think of the incoming radiation as being represented by a beam of photons, we need only consider the scattering of a quantum of energy $E = h\nu$ from a free electron; then, because of energy–momentum conservation, the scattered quantum has energy $E' = h\nu' < E$, in complete agreement with the experiments of Compton.

The frequency shift will depend on the angle of scattering and can be easily calculated from the kinematics. Consider an incoming photon of energy $E = h\nu$ and momentum $h\nu/c$ (Fig. 9.2) scattering from an electron (at rest) of mass m; p is the momentum of the electron after scattering, and $h\nu'$ and $h\nu'/c$ are the energy and momentum of the photon after the scattering. The three vectors $h\nu/c$, $h\nu'/c$, p must lie on the same plane, and energy conservation yields

$$h\nu + mc^2 = h\nu' + \sqrt{p^2c^2 + m^2c^4}. \tag{9.4}$$

From momentum conservation we obtain

$$h\nu = h\nu' \cos\theta + cp\cos\phi \tag{9.5}$$

$$0 = h\nu' \sin\theta - cp\sin\phi. \tag{9.6}$$

[1] See, for example, J. D. Jackson, *Classical Electrodynamics*, 3rd ed., p. 694, Wiley, New York, 1999.

Here θ is the photon scattering angle, and ϕ the electron recoil angle. To solve the above equations we transpose appropriately, square, and add Eq. (9.5) and Eq. (9.6) to obtain

$$h^2\nu^2 - 2h^2\nu\nu' \cos\theta + h^2\nu'^2 = c^2p^2.$$

By squaring Eq. (9.4) we obtain

$$h^2\nu^2 + h^2\nu'^2 - 2h^2\nu\nu' + 2hmc^2(\nu - \nu') = c^2p^2,$$

and substraction of the two above expressions yields

$$\frac{\nu - \nu'}{\nu\nu'} = \frac{h}{mc^2}(1 - \cos\theta). \tag{9.7}$$

We can recast Eq. (9.7) into two more familiar forms: (a) to give the shift in wavelength of the scattered X-ray beam

$$\Delta\lambda = \lambda' - \lambda = \frac{h}{mc}(1 - \cos\theta) \tag{9.8}$$

or (b) to give the energy of the scattered photon

$$E' = \frac{E}{1 + (E/mc^2)(1 - \cos\theta)}. \tag{9.9}$$

From Eq. (9.8) we see that the shift in wavelength, except for the angular dependence, is a constant, the Compton wavelength[2]

$$h/mc = 2.42 \times 10^{-10}\ \text{cm} = 0.0242\ \text{Å}.$$

For low-energy photons, with $\lambda \gg 0.02$ Å, the Compton shift is very small, whereas for high-energy photons with $\lambda \ll 0.02$ Å, the wavelength of the *scattered* radiation is always on the order of 0.02 Å, the Compton wavelength. These conclusions can equally well be obtained from Eq. (9.9), where the energy shift increases when E/mc^2 becomes large. For $E/mc^2 \gg 1$, E' is independent of E and on the order of $E' \approx mc^2$. Hence $\lambda' = c/\nu' = c/(E'/h) \sim c/(mc^2/h) = h/mc$ as stated before.

As an example, in this laboratory gamma rays from ^{137}Cs are scattered from an aluminum target; since $E = 0.662$ MeV, we have $E/mc^2 = 1.29$, so that backscattered gamma rays ($\theta = 180°$) will have $E' = E/3.6$,

[2] The mass of the electron m_e was used in evaluating h/mc; by using the mass of the pion, or another particle, we obtain the pion Compton wavelength, and so forth.

which is less than 30% of their original energy. It thus becomes quite easy to observe the Compton energy shift as compared to X-ray scattering, where, if we assume $\lambda = 2$ Å, $\Delta\lambda/\lambda = \Delta E/E = 0.01$.

In the original experiments Compton and his collaborators observed (especially for high Z materials) in addition to the frequency-shifted X-rays, scattered radiation *not shifted* in frequency. The unshifted X-rays are due to scattering from electrons that remained bound in the atom[3]: in this process the recoiling system is the entire atom, and we replace in Eq. (9.8) m by m_A (where $m_A \approx 2000 \times A \times m_e$), resulting in an undetectable wavelength shift, $\Delta\lambda' \approx 10^{-7}$ Å.

Next we are interested in the differential cross section for the scattering of the radiation from the electrons. Classically this is given by the Thomson cross section,[4] which can be easily derived: consider a plane wave propagating in the z direction with the **E** vector linearly polarized along the x direction. This is incident on an electron of mass m, as shown in Fig. 9.3. The electron will experience a force $F = eE = eE_0 \cos\omega t$, and its acceleration will be

$$\dot{v} = \frac{eE_0}{m}\cos\omega t.$$

According to Eq. (8.27), the power radiated by this accelerated electron will be (nonrelativistically, in SI units)

$$\frac{dP}{d\Omega} = \frac{1}{4\pi}\frac{e^2}{4\pi\epsilon_0}\frac{1}{c^3}\dot{v}^2\sin^2\Theta, \tag{9.10}$$

where Θ is the angle between the direction of observation and the **E** vector of the incoming wave. Using the expression for $\dot{v}$, we can write for Eq. (9.10) averaged over one cycle

$$\left\langle\frac{dP}{d\Omega}\right\rangle = \frac{1}{2}\left(\frac{e^2}{4\pi\epsilon_0 mc^2}\right)^2 \epsilon_0 E_0^2 c\sin^2\Theta.$$

Finally, from the definition of the cross section (see Section 8.2.1.a) we have

$$\frac{d\sigma}{d\Omega} = \frac{\text{energy radiated/(unit time} - \text{unit solid angle)}}{\text{incident energy/(unit area} - \text{unit time)}}.$$

[3] A similar situation is discussed in the following section on the Mössbauer effect, where the nucleus remains bound in the lattice and the recoiling system is the entire crystal.

[4] See also Section 8.2.5.

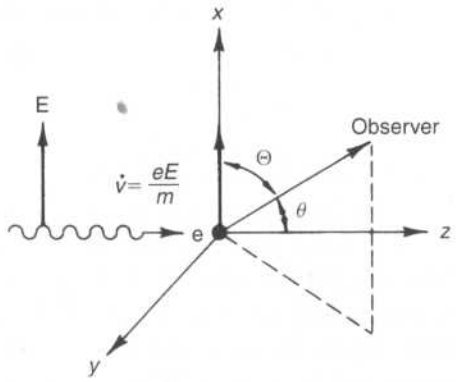

FIGURE 9.3 Classical picture of the scattering of electromagnetic radiation by an electron; this leads to the Thomson cross section.

Here the denominator is clearly given by the Poynting vector

$$\langle I\rangle = \frac{1}{2}\sqrt{\frac{\epsilon_0}{\mu_0}}E_0^2 = \frac{1}{2}\epsilon_0 cE_0^2.$$

Thus we obtain

$$\frac{d\sigma}{d\Omega} = \left(\frac{e^2}{4\pi\epsilon_0 mc^2}\right)^2 \sin^2\Theta, \tag{9.11}$$

where

$$\frac{e^2}{4\pi\epsilon_0 mc^2} = r_0$$

has dimensions of length, and is referred to as the "classical electron radius"

$$r_0 = 2.82 \times 10^{-13}\ \text{cm}.$$

Finally, we average over all possible directions of polarization of the incoming wave and use the angle θ measured from the direction of propagation of the incident wave to obtain

$$\frac{d\sigma}{d\Omega} = r_0^2\left(\frac{1+\cos^2\theta}{2}\right). \tag{9.12}$$

When integrated over all angles, Eq. (9.12) yields the Thomson cross section

$$\sigma_T = \frac{8\pi}{3} r_0^2. \tag{9.13}$$

(This result was given without proof in Eq. (8.21).)

Several objections can be raised to the simple cross section given by Eq. (9.12) or Eq. (9.13): (a) it does not depend on frequency, a fact not supported by experiment; (b) the electron, even though free, is assumed not to recoil; (c) the treatment is nonrelativistic; and (d) quantum effects are not taken into account. Indeed, the correct quantum-mechanical calculation for Compton scattering yields the so called Klein–Nishina formula[5]

$$\frac{d\sigma}{d\Omega} = r_0^2 \frac{1+\cos^2\theta}{2} \frac{1}{[1+\gamma(1-\cos\theta)]^2} \times \left[1 + \frac{\gamma^2(1-\cos\theta)^2}{(1+\cos^2\theta)[1+\gamma(1-\cos\theta)]}\right], \tag{9.14}$$

where r_0 and θ were defined previously, and $\gamma = h\nu/mc^2$. The cross section has been averaged over incoming (and summed over outgoing) polarizations. By integrating Eq. (9.14), the total cross section can be obtained. We will not give the complete result here, but the asymptotic expressions have already been presented in Eq. (8.22).

A comparison of the Thomson (Eq. (9.12)) and Klein–Nishina cross sections, including the results obtained in this laboratory for $\gamma = 1.29$, is shown in Fig. 9.8. We remark that although the Thomson cross section is symmetric about 90°, the Klein–Nishina cross section is peaked forward strongly as γ increases. This is due to a great extent to kinematical factors associated with the Lorentz transformation from the center of mass to the laboratory; note that the center-of-mass velocity of the (indicent gamma ray + free electron) system is

$$\bar{v} = c\bar{\beta} = c\gamma/(1+\gamma),$$

where as before $\gamma = h\nu/mc^2$.

The experimental data are in perfect agreement with the results of Eqs. (9.9) and (9.14), which are among the most impressive and convincing

[5] See for instance F. Gross, *Relativistic Quantum Mechanics and Field Theory*, Section 10.5, Wiley, New York, 1993.

successes of quantum theory. In the following two sections we will describe the experimental verification of these predictions.

9.2.2. The Compton Scattering Experiment

As with any scattering experiment, the apparatus will consist of:

(a) The beam of incident particles, in this case photons,
(b) The target (containing the electrons from which the photons scatter), and
(c) The detector of the scattered photons.

The beam of photons is obtained by collimating the gamma radiation from a ^{137}Cs source. An intense source is required in order to get an appreciable counting rate for the scattered photons. As shown in Fig. 8.21 ^{137}Cs (^{137}Ba) emits a gamma ray of energy 0.662 MeV, and the detection techniques have been discussed in Chapter 8. Figure 8.21 also shows the pulse-height spectrum of the gamma radiation from ^{137}Cs, as obtained with standard equipment; the same detection equipment is used in this experiment with the only difference that heavy shielding is needed to prevent the detector from seeing the intense ^{137}Cs source directly.

A schematic of the apparatus is shown in Fig. 9.4. The lead pig A is fixed and holds the source, which can be introduced through the vertical hole (V). Another lead shield B contains the detector and can be rotated about the center, where the target is located. The lead assemblies are rather heavy (approximately 100 lb) and some provisions must be taken for adequate mounting.

For the source, a 7-mCi ^{137}Cs sample was used, which was properly encapsulated before being shipped to the laboratory. It should always be transported in a lead container, and when transferred into the lead pig A, it must be handled only by the attached string. The source holder (A) has a collimator (h) drilled horizontally, subtending a solid angle on the order of 0.03 sr. Of interest to us will be the density of the photon beam at the target, and the *expected* value is

$$\frac{3.7\times10^{10}\times0.007}{4\pi}\frac{1}{r^2} = 1.3\times10^4 \text{ photons/cm}^2\text{-s},$$

where we use a source-to-detector distance $r = 40$ cm, for the data presented here.